The Interaction of Phe472 with a Fluorescent Inhibitor Bound to the Complex of Myosin Subfragment-1 with Nucleotide

Toshiaki Hiratsuka‡

The Department of Chemistry, Asahikawa Medical College, Asahikawa 078-8510, Japan

Received July 14, 2005; Revised Manuscript Received October 10, 2005

ABSTRACT: The fluorescent probe 3-[4-(3-phenyl-2-pyrazolin-1-yl)benzene-1-sulfonyl amido]phenylboronic acid (PPBA) acts as a fluorescent inhibitor for the ATPases of skeletal [Hiratsuka (1994) *J. Biol. Chem. 269,* 27251−27257] and *Dictyostelium discoideum* [Bobkov et al. (1997) *J. Muscle Res. Cell Motil. 18,* 563−571] myosins. The former paper suggested that, upon addition of excess nucleotides to the binary complex of subfragment-1 from skeletal myosin (S1) with PPBA, a stable ternary complex of S1 with PPBA and nucleotide is formed. Useful fluorescence properties of PPBA enable us to distinguish the conformation of the myosin ATPase at the ATP state from that at the ADP state. In the present paper, to determine the PPBA-binding site in the complexes, enzymatic and fluorescence properties of the S1·PPBA·nucleotide complexes were investigated. Upon formation of the ternary complex with ATP, a new peak appeared at 398 nm in the PPBA fluorescence spectrum. Experiments using model compounds of aromatic amino acid suggested that this fluorescence peak at 398 nm is originated from PPBA interacting with Phe residue(s). Taking into account differences in fluorescence spectra between complexes of S1 and those of subfragment-1 from *D. discoideum* myosin (S1dC), in the ternary complex of S1 formed with ATP, PPBA was suggested to interact with Phe residue(s) that is absent in S1dC. Docking simulation of PPBA on the S1·nucleotide complex revealed that Phe472 interacts with PPBA. Binding sites of PPBA and blebbistatin, an inhibitor showing high affinity and selectivity toward myosin II [Kovács et al. (2004) *J. Biol. Chem. 279,* 35557−35563], seem to overlap at least partly.

It has been reported that several synthetic dyes including fluorescent probes, not closely related to the structures of nucleotides, bind at the nucleotide site of enzymes and act as inhibitors (*1*−*4*). Inspection of literature reveals that apart from nucleotide analogues such compounds are, in general, aromatic molecules, frequently with negative charges attached to the aromatic ring system. X-ray crystallographic studies of such enzyme−inhibitor complexes of lactate dehydrogenase (*2*), alcohol dehydrogenase (*3*), and glycogen synthase kinase 3β (*4*) have revealed that the phenyl ring of inhibitor binds in the same hydrophobic pocket in which the adenosine moiety of the nucleotide binds. The utility of these compounds can be attributed primarily to the sensitivity of their spectroscopic properties to environment perturbations. Especially the use of fluorescent derivatives is of value in detecting transient in the enzymatic catalysis, in determining polarity of the nucleotide-binding pocket, and in studying the stereochemical and structural properties of the binding site. This is also the case for the fluorescent probe PPBA[1] for ATPases of S1 (*5*, *6*) and S1dC (*7*). PPBA, which binds noncovalently and stoichiometrically to S1, acts as an ATP-competitive inhibitor for the S1 and S1dC ATPases with K_i values of 0.8 and 1.6 μM, respectively.

Upon addition of excess nucleotides to the binary complex of PPBA·S1, the slow increase in fluorescence of PPBA is observed. It was suggested that this process consists of relatively fast equilibrium binding followed by a slow isomerization step of the complex (*5*). The scheme is as follows:

Scheme 1:

$$\mathrm{M{\cdot}PPBA} + \mathrm{N} \underset{k_{-1}}{\overset{k_1}{\rightleftharpoons}} \mathrm{M{\cdot}PPBA{\cdot}N} \underset{k_{-2}}{\overset{k_2}{\rightleftharpoons}} \mathrm{M^{*}{\cdot}PPBA{\cdot}N}$$

where M, N, and M*·PPBA·N represent S1, nucleotides or nucleotide analogues, and a stable ternary complex having different fluorescent properties, respectively. Since PPBA fluorescence is very sensitive to the state of the nucleotide-binding pocket, the fluorescence spectrum of the stable ternary complex formed with ATP is easily distinguishable from that of the complex with ADP. Thus fluorescence from the bound PPBA is very useful to monitor the conformational changes of S1 and S1dC during ATP hydrolysis (*5*−*7*). However, the assignment of the PPBA-binding site in stable ternary complexes has yet not been done not only with S1 but also with S1dC.

In the present paper, enzymatic and fluorescence properties of the ternary complexes of S1 were characterized to assign

‡ Mailing address: Department of Chemistry, Asahikawa Medical College, Midorigaoka higashi 2-1-1-1, Asahikawa 078-8510, Japan. Phone and fax: +81-166-68-2782. E-mail: toshiaki@asahikawa-med.ac.jp.

[1] Abbreviations: S1 and S1dC, subfragment-1 from skeletal and *Dictyostelium discoideum* myosins, respectively; PPBA, 3-[4-(3-phenyl-2-pyrazolin-1-yl)benzene-1-sulfonylamido]phenylboronic acid; AMP-PNP, adenyl-5′-yl imidodiphosphate; TNP-ADP, 2′,3′-*O*-(2,4,6-trinitrocyclohexadienylidene)-ADP; MOPS, 3-(*N*-morpholino)propanesulfonic acid; SA, serum albumin; BLG, β-lactoglobulin; V_i, orthovanadate; P_i, inorganic phosphate.

10.1021/bi051373l CCC: $33.50
Published on Web 01/04/2006

the PPBA-binding site. Fluorescence measurements of PPBA and Trp residues in the ternary complex formed with ATP suggested that PPBA is situated in the aqueous cavity near the bottom of the 50-kDa cleft, interacting with Phe472. Thus PPBA was proved to be useful fluorescent probe to detect conformational changes in the 50-kDa cleft of S1.

EXPERIMENTAL PROCEDURES

Materials. PPBA was purchased from Polysciences, Inc. AMP-PNP, BLG (from bovine milk), and SA (from bovine) were from Sigma. ATP and ADP were from Kohjin Co. Other reagents were of reagent or biochemical research grade. S1 was prepared by chymotryptic digestion of skeletal myosin (*8*). TNP-ADP, S1·TNP-ADP· V_i, and S1·ADP·V_i were prepared as previously described (*9*, *10*). The isolated complexes, in which 0.85 and 0.94 mol of TNP-ADP and ADP per mole of S1, respectively, had been trapped, were used for experiments.

Buffer System. Except for ATPase measurements, all experiments with protein samples were carried out in 40 mM MOPS, pH 7.0, 30 mM KCl, and 2 mM $MgCl_2$. Because PPBA is scarcely soluble in water, all reaction mixtures with protein and PPBA contained 0.4% *N*,*N*-dimethylformamide as previously described (*5*).

Fluorescence Measurements. Fluorescence measurements were carried out at 25 °C in a thermostated Hitachi fluorescence spectrophotometer model F-4010 as previously described (*5*), excited at 290 and 360 nm for Trp and PPBA fluorescence, respectively. Only when spectra of PPBA were recorded in phenol compounds, measurements were carried out at 45 °C, since their freezing points are 40−41 °C. A control experiment with PPBA in *N*,*N*-dimethylformamide showed that there is no difference in shapes between spectra at 45 °C and 25 °C. All fluorescence emission and excitation spectra of PPBA in the presence and absence of S1 were corrected. The emission spectra derived from PPBA bound to S1 were obtained by subtracting the spectrum of unbound PPBA from the overall spectrum, using dissociation constants of 26, 0.8, 2.6, and 3.3 μM for PPBA bound to S1 in the binary complex and the ternary complexes with ATP, AMP-PNP, and ADP, respectively (*5*). The numbers of PPBA-binding sites on S1 and the dissociation constants were calculated by Scatchard analysis as previously described (*5*).

ATPase Measurements. Measurements of ATPase activity were carried out in 40 mM MOPS, pH 7.0, 18 mM KCl, and 2 mM $MgCl_2$ at 25 °C. P_i liberated was determined as previously described (*5*).

Molecular Modeling. Structural models of S1dC and S1 were constructed by using coordinates in the Brookhaven Protein Data Bank (1MND and 2MYS, respectively) (*11*, *12*). For the molecular structure of ATP the coordinate of ATP bound to S1 (1FMW) (*13*) was used. The conformations of PPBA and blebbistatin were analyzed by molecular mechanics using semiempirical quantum method AM1 (*14*) implemented in the program MOPAC 97 module of ChemBats3D Ultra v.5.0 (Cambridge Soft, Cambridge, MA). The geometric optimization is characterized by a minimization of the force constants. The energy-minimized structure of PPBA was fitted into S1dC following manual superposition using the program Swiss-PdbViewer 3.6b2. The initial model was then submitted to this program in the "Energy Minimization", which generated a refined, energy-minimized structure of the ternary complex using Gromos96. Structural diagrams of protein were generated using the program WebLab Viewer (Accelrys Inc., San Diego, CA).

RESULTS AND DISCUSSION

Properties of Ternary Complexes of S1·PPBA·Nucleotide. It is well-known that V_i for the myosin ATPase (*15*) and the metal(III)·ATP complexes for hexokinase (*16*) as analogues of P_i and Mg^{2+}·ATP, respectively, are the so-called slow-binding inhibitors (*17*). Slow-binding inhibitors are such good analogues of the substrate that they induce a conformational change in the enzyme which is analogous to that associated with the formation of the transition state in enzymatic catalysis (*17*). The forward isomerization reaction would then be slow because the inhibitor does not have all the essential structural features of the transition state of a substrate. Thus, the onset of the inhibition during enzymatic assay is slow. When a reaction, in the presence of inhibitor, is started by the addition of enzyme, the relatively rapid initial velocity decreases to a slower steady state rate (*15*, *17*). On the other hand, the analysis of the initial rate shows that the inhibitor acts as a competitive inhibitor for the enzyme (*16*). This is also the case for PPBA. The analysis of the initial rate of the S1 ATPase in the presence of PPBA showed that PPBA competes with ATP (*5*). When the Mg^{2+}-ATPase reaction was started by adding S1 to the reaction mixture containing ATP and PPBA, the relatively rapid initial velocity decreased to a slower steady state rate (not shown). In the presence of 3 μM PPBA, the slower steady state rate was about 40% of the initial rate. Thus, PPBA is a slow-binding inhibitor for the myosin ATPase as well as V_i (see below).

In the case of V_i, the source of the slow inhibition consists of the formation of a stable, inactive ternary complex with the composition of the myosin ATPase, V_i, and ADP (*15*). Thus, it was suggested that the slow inhibition observed with PPBA results from the formation of a stable, inactive ternary complex with PPBA, S1, and nucleotide (Scheme 1). To obtain information about the ternary complex, I investigated properties of the complex formed with ATP. The formation of the ternary complex was initiated by the addition of excess ATP to the binary complex of S1 with PPBA (Figure 1A). The complex formation was accompanied by a large increase in PPBA fluorescence at 400 nm in agreement with the previous result (*5*). The first-order rate constant of the formation of the ternary complex was obtained to be 6.1×10^{-3} s^{-1}.

As shown in Figure 1A (inset), the Mg^{2+}-ATPase activity of S1 gradually decreased with increasing amount of PPBA bound. Extrapolation to a complete inactivation indicated that the loss of activity correlates with formation of the ternary complex in which 1.1 mol of PPBA per mole of S1 binds. This result suggests that the stable ternary complex formed with S1, PPBA, and ATP has 1 mol of PPBA per mole of S1 and no ATPase activity.

PPBA was added after the complex formation of S1 with ATP. There was no significant difference in enzymatic and fluorescence properties between this sample and the sample prepared by the addition of PPBA prior to the formation of S1·ADP·P_i complex (not shown). Thus either addition

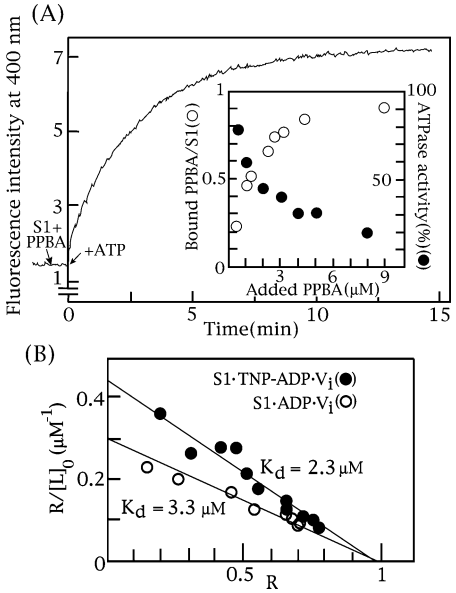

FIGURE 1: Formation of ternary complexes of S1 with PPBA and nucleotides. (A) Change in PPBA fluorescence of the S1·PPBA complex accompanied by ATP addition. Fluorescence change by the formation of the ternary complex was measured at 400 nm with S1 (1 μM), PPBA (3 μM), and ATP (0.2 mM). Inset: Changes in the amount of PPBA bound to S1 and the Mg^{2+}-ATPase activity of S1 as a function of concentration of PPBA added. S1 (1 μM) was mixed with various concentrations of PPBA (0.5−9 μM), followed by incubation with ATP (1 mM) for 30 min. Aliquots of the sample were subjected to measurements of the Mg^{2+}-ATPase activity and fluorescence spectrum. The amount of PPBA bound to S1 in the ternary complex was estimated from the increase in PPBA fluorescence as previously described (*5*). (B) Scatchard plots for the binding of PPBA (1 μM) to the isolated complexes (0.7−10 μM) of S1·ADP·V_i (○) and S1·TNP-ADP·V_i (●). R and $[L]_0$ are the moles of PPBA bound per mole of S1 and the concentration of free S1·nucleotide·V_i, respectively.

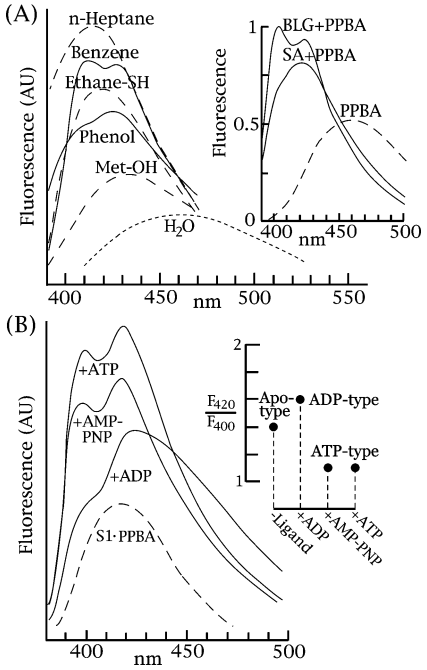

FIGURE 2: Fluorescence emission spectra of PPBA in organic solvents and bound to proteins. (A) Corrected fluorescence spectra of PPBA in various organic solvents as model compounds for amino acid residues. Spectra of PPBA (0.8 μM) were measured in methanol, ethanethiol, *n*-heptane, phenol, and benzene. Inset: Corrected fluorescence emission spectra of PPBA bound to BLG and SA. PPBA (1 μM) was mixed with BLG (47 μM) and SA (46 μM), followed by fluorescence measurements. Under this condition, 95% and 97% of the added PPBA bind to BLG and SA, respectively. (B) Corrected fluorescence emission spectra of PPBA bound to S1 in the binary (− − −) and the ternary (—) complexes formed with ATP, AMP-PNP, and ADP. Spectra were obtained by subtracting the spectrum of unbound PPBA from the overall spectrum as described in Experimental Procedures. Inset: F_{420nm}/F_{400nm} ratios of fluorescence spectra of PPBA bound to S1. The values were calculated from spectra in part B.

generates the same ternary complex, excluding possible artifacts of PPBA binding to S1.

Dissociation of the ternary complex formed with ATP was examined by extensive dialysis of the sample at 4 °C (not shown). A longer period of dialysis (about 3 days) was required for a complete dissociation of the complex. This result suggests that the ternary complex formed with S1, PPBA, and ATP is very stable, but the binding is in a noncovalent fashion.

To obtain information about the PPBA-binding site in the S1·PPBA·nucleotide complex, the PPBA complexes were prepared using isolated S1 complexes with ADP·V_i and TNP-ADP·V_i. As shown in Figure 1B, Scatchard analyses yielded the number of PPBA-binding sites and the dissociation constant of PPBA for the two complexes. With the S1·TNP-ADP·V_i complex, the number of PPBA-binding sites and the dissociation constant were calculated to be 1.0/mol of S1 and 2.3 μM, respectively. With the S1·ADP·V_i complex, similar values (1.0/mol of S1 and 3.3 μM, respectively) were obtained. These values were comparable to those (1.0/mol of S1 and 0.8−3.3 μM, respectively) obtained with the ternary complexes formed with ATP, ADP, and AMP-PNP (*5*).

When PPBA was added to the complex of S1·TNP-ADP·V_i, the fluorescence spectrum originated from TNP-ADP (500−600 nm) remained unchanged during the course of formation of the PPBA complex (not shown). This result indicates that, upon formation of the PPBA complex, PPBA not only dissociates TNP-ADP from S1 but also affects the state of TNP-ADP bound. Thus, upon binding of PPBA to the S1·nucleotide complex, PPBA seems to enter the PPBA-binding site other than the ATP-binding pocket directly, resulting in the formation of the stable ternary complex of PPBA·S1·nucleotide (Scheme 1).

Fluorescence Spectra of PPBA Interacting with Phe and Tyr. It has been reported that the fluorescence intensity and the position of the emission maximum in the fluorescence spectrum of PPBA vary significantly with solvent polarity (*5*). To obtain further information about fluorescence properties of PPBA, I measured corrected fluorescence spectra of PPBA in various organic solvents as models of PPBA interacting with various amino acids, especially hydrophobic ones (Figure 2A).

Nonaromatic solvents methanol, ethanethiol, and *n*-heptane were used as model compounds of Ser/Thr, Cys/Met, and Val/Ile/Ala, respectively. The emission maximum of PPBA was shifted from 460 nm in water to 432 nm in methanol, 419 nm in ethanethiol, and 416 nm in *n*-heptane. All the spectra showed a single emission maximum without a shoulder. This was also the case for measurements with *N*,*N*-dimethylformamide, dimethyl sulfoxide, ethanol, 1-butanol, and chloroform (not shown). It should be noted that, whenever nonaromatic organic solvents are used, the spec-

trum with a single emission maximum without a shoulder is obtained.

The spectra of PPBA measured in aromatic solvents were different from those of PPBA in nonaromatic solvents. With benzene as a model compound of Phe, the spectrum showed two emission maxima at 409 and 424 nm. This spectrum coincided with those measured in toluene and 4-chlorotoluene (not shown). However, with phenol as a model compound of Tyr, only one emission maximum was observed at 422 nm. Unlike benzene, phenol gave no emission maximum around 400 nm but only a shoulder. This was also the case for the spectrum measured in 2-chlorophenol (not shown).

The fluorescence emission maxima of PPBA were plotted against the dielectric constant of the solvent (not shown). The maxima were found to vary over a wide range, and to be correlated with the polarity of the solvent: increasing polarity led to longer wavelength. However, only in aromatic solvents, benzene, toluene, 4-chlorotoluene, phenol, and 2-chlorophenol, the emission maxima of PPBA clearly lay outside the observed correlation. Together with the result shown in Figure 2A, this behavior should therefore be attributed to properties of the aromatic solvent other than its polarity (*18*). It is highly likely that PPBA interacts with the aromatic ring of solvent.

In order to confirm this point, I measured fluorescence spectra of PPBA bound to model proteins. BLG and SA have a single ligand site as the primary binding site. Fluorescent probes such as anilino- and dimethylanilino-naphthalene sulfonates show specificity toward these ligand-binding sites (*19*, *20*). This is also the case for PPBA. PPBA was found to bind firmly to BLG and SA as well as S1, accompanied by a large fluorescence increase. Scatchard analyses for the binding of PPBA to BLG and SA yielded linear plots (not shown). For BLG, the number of PPBA-binding sites and the dissociation constant were calculated to be 1.0/mol of protein and 3.9 μM, respectively. Similar values (0.94/mol of protein and 1.6 μM, respectively) were obtained with SA.

It is well established that aromatic residues located at ligand-binding sites of these proteins (Phe105 in BLG and Tyr411 in SA) interact with the ligand bound (*21*, *22*). This makes BLG and SA suitable model proteins. The spectrum of PPBA bound to BLG showed two maxima at 403 and 423 nm (Figure 2A, inset), resembling that of PPBA in benzene and toluene with two maxima at 409 and 424 nm (Figure 2A). However, the spectrum of PPBA bound to SA showed no emission maximum around 400 nm. It showed a shoulder around 400 nm and a maximum at 421 nm, resembling that of PPBA measured in phenol with a shoulder around 400 nm and a maximum at 422 nm.

This result is consistent with ligands bound to the ligand-binding sites in BLG and SA interacting with Phe105 and Tyr411, respectively (*21*, *22*). Thus, the interaction of PPBA with Phe residue(s) in proteins is distinguishable from that with all other residues. The coexistence of two emission maxima around 400 and 420 nm in the fluorescence spectrum of the PPBA·protein complex is an indication of the PPBA−Phe interaction.

Fluorescence Spectra of PPBA in S1 Complexes. Figure 2B shows fluorescence spectra of PPBA in the binary and ternary complexes of S1. All spectra were obtained by subtracting the spectrum of unbound PPBA from the overall spectrum. The S1·PPBA complex shows the spectrum with a single emission maximum at 418 nm. On the other hand, the spectra of the ternary complexes were different from that of the binary complex. The spectrum of the S1·PPBA·ADP complex has a maximum at 424 nm and a shoulder around 400 nm. The spectrum of the ternary complex formed with ATP was essentially identical to that of the complex with AMP-PNP. However, both spectra were distinct from that of the complex with ADP, showing two maxima at 398 and 419 nm. According to F_{420nm}/F_{400nm} ratios of complexes, fluorescence spectra of PPBA in S1 complexes were classified into three types: apo-, ADP-, and ATP-types. The F_{420nm}/F_{400nm} ratios were 1.4, 1.6, and 1.1, respectively (Figure 2B, inset).

Taking into consideration the results of model experiments (Figure 2A), the spectrum of PPBA measured in benzene resembled only the ATP-type spectrum in the shape and position of the emission maxima. This result suggests that PPBA bound to S1 interacts with the Phe residue(s) at the ADP·P_i state but does not at the apo and ADP states.

It has been reported that PPBA binds noncovalently and stoichiometrically to S1dC as well as S1 (*7*). Furthermore, PPBA acts as an ATP-competitive inhibitor for the S1dC ATPase with a K_i value of 1.6 μM, which is similar to the value of S1 ATPase (0.8 μM) (*5*). There is no significant difference in properties for the interaction with PPBA between S1dC and S1 (*7*). However, no fluorescence increase at 400 nm, which is an indication of the PPBA-Phe interaction in the complex of S1 (Figures 1A and 2B), is observed upon formation of the ternary complex of S1dC with ATP and the analogues. This suggests that the Phe residue(s) interacting with PPBA at the ADP·P_i state in S1 is absent in S1dC.

Effects of PPBA on Trp Fluorescence of S1. Enhancement of Trp fluorescence upon ATP binding to S1 is a good indicator of conformational change (*23*). S1 contains five Trp residues positioned at 113, 131, 440, 510, and 595. Trp510 has been identified to be the primary ATP-sensitive Trp residue (*24*−*29*). Next I checked if the PPBA-binding affects Trp fluorescence of S1. A control experiment showed that the addition of ATP, AMP-PNP, and ADP in the absence of PPBA results in an increase in S1 fluorescence by 17%, 12%, and 3%, respectively (Figure 3A). AMP had no effect on S1 fluorescence. The addition of PPBA alone caused a small increase (2%) in S1 fluorescence (Figure 3B).

When ATP and AMP-PNP were added to the S1·PPBA complex, the initial increase in S1 fluorescence was followed by a quenching phase (Figure 3B). Finally fluorescence intensities leveled off with 95 (for ATP) and 102% (for AMP-PNP) values of S1 alone. However, in the case of the complex with ADP, the subsequent quenching of S1 fluorescence scarcely occurred. AMP had no effect again on fluorescence of S1 with PPBA.

The ATP-induced quenching of Trp fluorescence in the S1·PPBA complex was accelerated with increasing amounts of PPBA added (Figure 3C, inset). The quenching rate obeyed good first-order kinetics, indicating no dependence on difference in their initial fluorescence intensities. The observed rate constant for the quenching of Trp fluorescence was correlated well with the amount of PPBA bound to S1 (Figure 3C), suggesting that only S1 bound by PPBA is responsible for the fluorescence quenching.

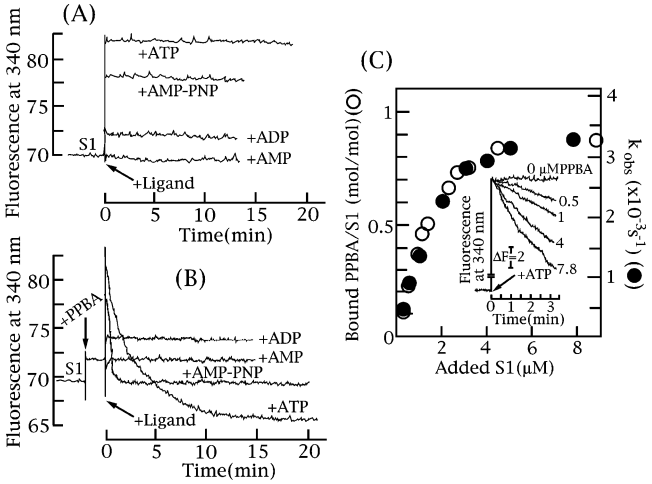

FIGURE 3: Effects of PPBA binding on the Trp fluorescence of S1. Nucleotide-induced changes in Trp fluorescence of S1 (A) and the S1·PPBA complex (B) were measured. Nucleotides and AMP-PNP (1 mM) were mixed with S1 (1 μM) in the presence and absence of PPBA (3 μM). (C) A correlation between the rate constant for Trp fluorescence quenching and the amount of PPBA bound to S1. The rate constant k was obtained from the firs-order plots of data in the inset. The amount of PPBA bound to S1 was determined from the increase in PPBA fluorescence (*5*). Inset: Changes in Trp fluorescence of S1 in the presence of various concentrations of PPBA accompanied by the ATP addition. ATP (20 μM) was mixed with S1 (1 μM) in the presence of PPBA (0−7.8 μM). For all samples, the fluorescence intensity of the S1·PPBA complex in the absence of ATP was normalized to that of S1 alone.

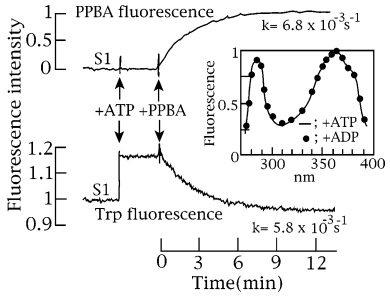

FIGURE 4: Simultaneous occurrence of quenching in the Trp fluorescence and enhancement in the PPBA fluorescence upon formation of the ternary complex. ATP (1 mM) and PPBA (3 μM) were mixed with S1 (1 μM). Fluorescence of PPBA and Trp was measured at 400 and 340 nm, respectively. Inset: Corrected excitation spectra of ternary complexes formed with ADP (●) and ATP (—). Fluorescence intensity was normalized to 1 at 363 nm to give the same apparent PPBA concentration for two samples. The spectra were recorded with the emission wavelength at 400 nm under the same condition as in Figure 3B at a time when the constant value for the extent of quenching was reached (15−20 min after addition of nucleotides).

As shown in Figure 1A, the formation of the stable ternary complex with ATP causes an increase in PPBA fluorescence at 400 nm, which is originated from the PPBA−Phe interaction (Figure 2B). Thus I compared the time course of increase in PPBA fluorescence (Figure 1A) with that of quenching of Trp fluorescence of S1 (Figure 3B) upon formation of the ternary complex. Since the ATP-induced quenching of Trp fluorescence in the S1·PPBA complex did not depend on the order of ATP addition, similar quenching was again observed in the case of the subsequent addition of PPBA to the complex of S1 with ATP. As shown in Figure 4, the data clearly show that the PPBA-induced quenching of Trp fluorescence and the increase in PPBA fluorescence

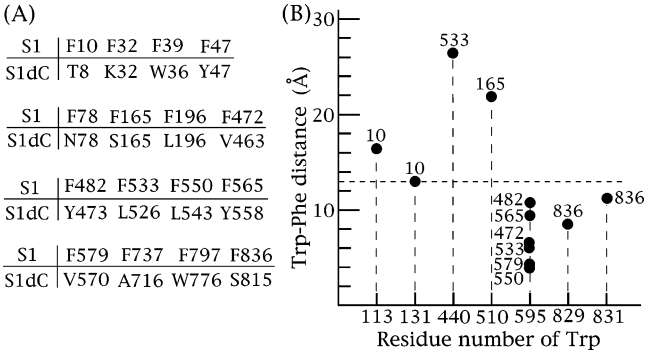

FIGURE 5: Assignment of Phe and Trp residues interacting with PPBA. (A) Phe residues in S1 that are replaced by other residues in S1dC. Corresponding residues in S1dC are also shown. (B) The closest distances (●) between Phe and Trp residues in the skeletal myosin head. Using the coordinate of S1 (2MYS), distance measurements were made only for Phe residues that are replaced by other residues in S1dC (A). Residue numbers of Phe and Trp residues in S1 are indicated near closed circles and on the abscissa, respectively. Only Trp-Phe pairs having distances within 30 Å are shown. A dotted line indicates the molecular length of PPBA (13 Å, see Figure 8B).

occur simultaneously with first-order rate constants of 5.8 and 6.8 $\times$ 10^{-3} s^{-1}, respectively, generating mirror images to each other's course.

To obtain further information about the quenching of Trp fluorescence, I compared the excitation spectrum of the complex of S1·PPBA·ADP·P_i with that of the complex of S1·PPBA·ADP. Figure 4 (inset) shows that there is no difference in the Trp component of the excitation spectrum (270−300 nm) between the two ternary complexes formed with ATP and ADP.

Assignment of the PPBA-Binding Site in Ternary Complexes. For the PPBA-binding site in ternary complexes of S1·PPBA·nucleotide, the assignment was made according to the following criteria: (1) the comparison of the fluorescence spectrum of the S1·PPBA·ADP·P_i complex with that of PPBA measured in benzene suggests that the bound PPBA interacts with Phe residue(s) (Figure 2A,B); and (2) this Phe residue(s) is absent in S1dC because the ternary complex of S1dC shows no fluorescence spectrum characteristic of the Phe−PPBA interaction (*7*).

Aromatic residues, especially Phe and Trp residues, are important components for the binding sites of hydrophobic ligands in proteins. The heavy chain of S1 contains 49 Phe residues. Among them, 16 Phe residues are absent in S1dC. Figure 5A shows these Phe residues together with the corresponding residues in S1dC. On the other hand, the skeletal myosin head contains 7 Trp residues positioned at 113, 131, 440, 510, 595, 829, and 831. To examine the possibility that Phe and Trp residues interact with PPBA at the same time, I measured the closest Trp−Phe distances for these 16 Phe and 7 Trp residues. Figure 5B shows such pairs with distances less than 30 Å.

Among these Trp residues, Trp829 and 831 should be excluded from the participation in the interaction with PPBA because they are located in the C-terminal of α-helical tail in S1 (*11*). Trp113 and 131, which are situated at the entrance of nucleotide-binding pocket (*12*), were also excluded. This is the reason why the present result with the use of the S1·TNP-ADP·V_i complex (Figure 1) suggested that the PPBA-binding site is not near the nucleotide-binding pocket of S1.

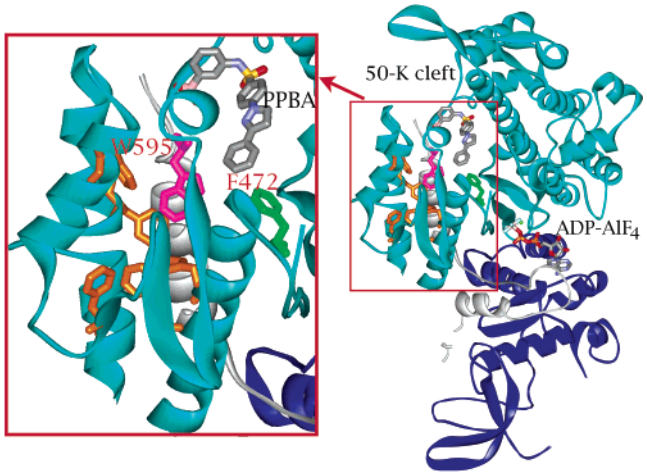

FIGURE 6: Proposed structure of the ternary complex of S1.The energy-minimized structure of the ternary complex formed with S1, PPBA, and ATP was obtained using the coordinate of the S1dC complex with ADP-AlF_4 (1MND) as described in Experimental Procedures. Overall structure of the ternary complex (right) and a close-up view of the PPBA-binding site (left) are shown. Peptide chains of 50- (residues 210−620), 25- (2−201), and 20-kDa (627−690) segments in S1 are in cyan, white, and blue, respectively. Trp595 (magenta), Phe472 (green), and Phe residues of 482, 533, 550, 565, and 579 (orange) are shown in sticks. PPBA and ADP-AlF_4 are in CPK color. Residue numbers are expressed as corresponding numbers of skeletal S1 (*12*). Val463 in S1dC is expressed as Phe472, the corresponding residue in S1.

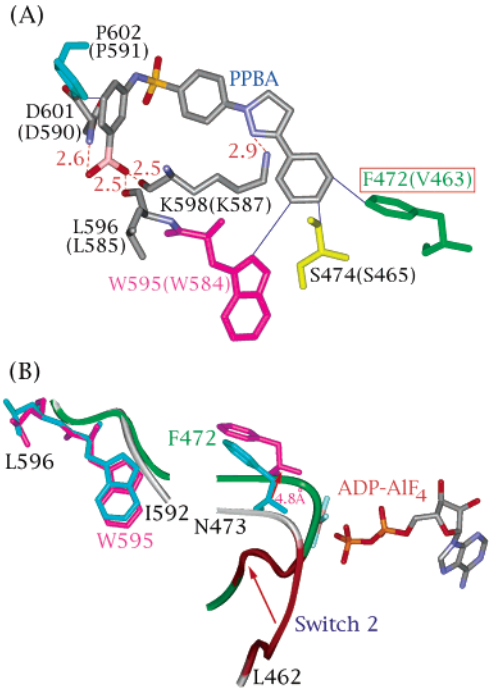

FIGURE 7: Environment around PPBA bound to S1. (A) Residues interacting with PPBA bound to S1. Hydrophobic residues with distances less than 5.5 Å from PPBA (Phe472, Ser474, Trp595, and Pro602) are in green, yellow, magenta, and cyan, respectively. PPBA and residues that form hydrogen bonds with PPBA (Leu596, Lys598, and Asp601) are in CPK color. Predicted van der Waals interactions and hydrogen bonds are expressed as blue solid and red dotted lines, respectively. Residue numbers in brackets indicate corresponding residues in S1dC. (B) Structures around Phe472 in S1 at apo and ADP·P_i states. Using coordinates of S1 (2MYS, for apo state) and S1dC (1MND, for ADP·P_i state), 3 atoms of S1 (Cα and N of Trp595, and Cα of Leu596) were superimposed onto the corresponding atoms of S1dC (Trp584 and Leu585), respectively. The switch 2 region is in red. Peptide chains (I592−L596 and L462−N473) except for the switch 2 region at apo and ADP·P_i states are white and green, respectively. Residues (Leu596, Trp595, and Phe472) at apo and ADP·P_i states are in cyan and magenta, respectively. Val463 in S1dC are expressed as the corresponding residue in S1 (Phe472). ADP-AlF_4 is in CPK color.

On the other hand, the closest Trp−Phe distances for Trp440 and 510 are 26 and 22 Å, respectively. These Trp and Phe residues are too far apart for PPBA to interact at the same time since the molecular length of PPBA is about 13 Å (Figure 8D). Thus, Trp440 and 510 were also excluded. Finally, Trp595 is the most probable as a candidate for the Trp residue interacting with PPBA in the ternary complex. For Trp595, all the closest Trp−Phe distances are less than 11 Å, which is less than the molecular length of PPBA (13 Å). It should be noted that Trp595 and all Phe residues positioned at 472, 482, 533, 550, 565, and 579 are located on the 50-kDa segment of S1 (*12*).

Molecular Modeling. I performed docking simulations of PPBA on the S1·nucleotide complex to elucidate the structural basis of the interaction of PPBA with Phe residue(s) that is absent in S1dC (Figure 5A). The energy-minimized structure of PPBA was initially determined using Chemdraw 3D Ultra v.5.0. Based on the criteria for the assignment of the PPBA-binding site described above, PPBA was then "fitted" into S1dC following manual superposition using Swiss-Pdb Viewer V.3.6b2. However, whenever PPBA interacts with any of the 15 Phe residues other than Phe472, there was no room to accommodate PPBA in S1 (not shown). Thus, the structure where Phe472 interacts with PPBA is the only possible structure for the ternary complex formed with S1, PPBA, and ATP. The energy of the resulting structure was then minimized using Gromos96, which generated a refined model for the ternary complex (Figure 6). In the model, PPBA binds to the aqueous cavity between the actin-binding cleft and the nucleotide-binding pocket of S1, and interacts with either Phe472 or Trp595. However, the PPBA-induced quenching of S1 fluorescence (Figure 3B) does not result from the interaction between PPBA and Trp595 because this residue is ATP-insensitive (27). It is highly likely that the binding of PPBA to S1 perturbs Trp510, and this perturbation eliminates the ATP sensitivity. As a result, the enhancement of S1 fluorescence is abolished.

In this fitting scenario, all van der Waals interactions are reasonable (Figure 7A). Phe472, Ser474, and Trp595 are positioned to interact with the ring *a* of the fluorophore moiety of PPBA (Figure 8B). Pro591 is in close proximity to the ring *d*. Furthermore, Leu596, Lys598, and Asp601 are well positioned to form hydrogen bonds with the boronate and fluorophore moieties of PPBA.

It has been reported that the so-called "switch 2 region" of S1 (Ile464−Asp471) is in a closed conformation at the ADP·P_i state while it is in an open one at ADP and apo states (*30*, *31*). As shown in Figure 7B, Phe472 is next to the end of the switch 2 region. It should be noted that this residue (Cα) moves about 4.8 Å between the ADP·P_i and apo states. Thus it is reasonable that PPBA detects difference in conformations between the two ternary complexes formed with ATP and ADP, showing different fluorescence spectra (Figure 2B). Of relevance to this suggestion, previous work (*5*) has shown that the PPBA-binding site in the ADP·P_i state

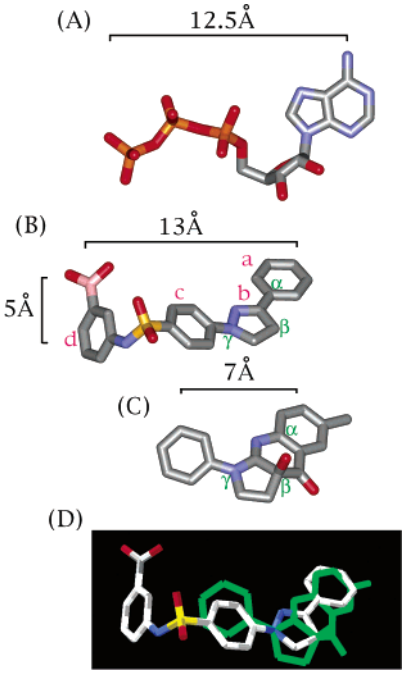

FIGURE 8: Structural comparison of PPBA, ATP, and blebbistatin. Energy-minimized conformations of PPBA (B) and blebbistatin (C) are obtained as described in Experimental Procedures. For the ATP conformation (A) the coodinate of ATP molecule bound to S1 (1FMW) was used. In part B, rings *a*−*c* and *d* indicate the fluorophore and phenyl boronate moieties, respectively. Carbon, nitrogen, oxygen, sulfur, phosphorus, and boron atoms are in gray, blue, red, yellow, orange, and pink, respectively. (D) Superposition of the fluorophore moiety of PPBA (CPK color) and blebbistatin (green), in which 3 atoms of PPBA (α−γ in part B) were superimposed onto the corresponding atoms of blebbistatin (α−γ in part C).

is more closed and/or tightened than those in the ADP and apo states.

Comparison of PPBA with ATP and Blebbistatin. Figures 8A and 8B show the structural models of ATP and PPBA, respectively. PPBA consists of mainly three aromatic rings (rings *a*, *c*, and *d*) and one heterocyclic ring (ring *b*) together with charged groups of the sulfonyl and the boronate (*5*). The fluorophore moiety of PPBA consists of rings *a*−*c*. The PPBA (about 13 Å) and ATP (about 12.5 Å) molecules are a similar size. I found some basic resemblances between the two structures. The comparison of structural molecular models of PPBA and ATP shows substantial structural correspondences, including precise alignments of the fluorophore moiety (rings *a*−*c*), the sulfonyl, and the boronate of PPBA with the adenosine moiety, the β-phosphoryl, and the γ-phosphoryl of ATP, respectively. Thus it is anticipated that the fluorophore of PPBA binds to the adenosine-binding site in the ATP-binding pocket of S1, and the charged groups of sulfonyl and boronate bind near residues, which are responsible for the formation of hydrogen bond to phosphoryl moieties of ATP. These structural features of PPBA seem to be the reason why PPBA acts as an ATP-competitive inhibitor for myosin ATPases (*5*−*7*).

Blebbistatin is a recently discovered inhibitor showing high affinity and selectivity toward myosin II (*32*). Although PPBA is larger than blebbistatin by about 6 Å, the size of its fluorophore moiety (rings *a*−*c*) is similar to that of blebbistatin (Figure 8B,C). Thus, blebbistatin is well superimposed on the fluorophore moiety of PPBA (Figure 8D). However, blebbistatin has no charged group unlike PPBA. This seems to be the reason why blebbistatin does not act as an ATP-competitive inhibitor for the myosin ATPase (*32*).

It is interesting to compare the effects of blebbistatin on S1 with those of PPBA on S1. When blebbistatin is added to S1 with ATP, the initial increase in Trp fluorescence is followed by a quenching phase leading to a steady state fluorescence level that is 5−10% lower than that of S1 alone (32). The quenching phase is a single exponential, and its rate constant is dependent on blebbistatin concentration. Similar results were obtained with PPBA (Figures 3 and 4). On the other hand, the blebbistatin binding is 8−10 times stronger in S1 at the ADP·P_i state than that at the apo state (32). This is also the case for PPBA (5). The PPBA binding is 33 times stronger in S1 at the ADP·P_i state than that at the apo state. These results suggest that effects of PPBA on S1 in ternary complexes are similar to those of blebbistatin on S1. Furthermore, it has been reported that blebbistatin binds to the cavity between the actin-binding cleft and the ATP-binding pocket of S1 (32) as well as PPBA (Figure 6). Thus, it is highly likely that binding sites of PPBA and blebbistatin overlap at least partly. The hydrophobic nature of the site, surrounded by Phe472, Ser474, and Trp595 (Figure 7A), is favorable for the binding of hydrophobic ligands.

In conclusion, PPBA is situated within the aqueous cavity between the actin-binding cleft and the ATP-binding pocket of S1 in the ternary complex formed with ATP. Fluorescence spectra of PPBA interacting with model compounds of amino acids reveal the interaction of PPBA with Phe472 in the 50-kDa segment of S1. These features make PPBA a useful fluorescent probe in the investigation of conformational changes in the 50-kDa cleft of S1.

REFERENCES

1. Neslund, G. G., Miara, J. E., Kang, J.-J., and Dahms, A. S. (1984) Specific Interactions of Xanthene Dyes with Nucleotide-Binding Sites of Membrane Energy-Transducing Enzymes and Carriers, *Curr. Top. Cell. Regul. 24*, 447−469.
2. Wassarman, P. M., and Lentz, P. J., Jr. (1971) The Interaction of Tetra-iodofluorescein with Dogfish Muscle Lactate Dehydrogenase: A Chemical and X-ray Crystallographic Study, *J. Mol. Biol. 60*, 509−522.
3. Einarsson, R., Eklund, H., Zeppezauer, E., Boiwe, T., and Brändén, C.-I. (1974) Binding of Salicylate in the Adenosine-Binding Pocket of Dehydrogenases, *Eur. J. Biochem. 49*, 41−47.
4. Bertrand, J. A., Thieffine, S., Vulpetti, A., Cristiani, C., Valsasina, B., Knapp, S., Kalisz, H. M., and Flocco, M. (2003) Structural Characterization of the GSK-3β Active Site Using Selective and Non-selective ATP-mimetic Inhibitors, *J. Mol. Biol. 333*, 393−407.
5. Hiratsuka, T. (1994) Nucleotide-induced Closure of the ATP-binding Pocket in Myosin Subfragment-1, *J. Biol. Chem. 269*, 27251−27257.
6. Bobkov, A. A., and Reisler, E. (2000) Is SH1-SH2-Cross-Linked Myosin Subfragment 1 a Structural Analog of the Weakly-Bound State of Myosin?, *Biophys. J. 79*, 460−467.
7. Bobkov, A. A., Sutoh, K., and Reisler, E. (1997) Nucleotide and actin binding properties of the isolated motor domain from *Dictyostelium discoideum* myosin, *J. Muscle Res. Cell Motil. 18*, 563−571.
8. Weeds, A. G. and Taylor, R. S. (1975) Separation of subfragment-1 isoenzymes from rabbit skeletal muscle myosin, *Nature 257*, 54−56.
9. Hiratsuka, T. (1982) Biological Activities and Spectroscopic Properties of Chromophoric and Fluorescene Analogs of Adenine Nucleoside and Nucleotides, 2′,3′-*O*-(2,4,6-Trinitrocyclohexadienylidene) Adenosine Derivatives, *Biochim. Biophys. Acta 719*, 509−517.

10. Hiratsuka, T. (1984) Affinity Labeling of the Myosin ATPase with Ribose-Modified Fluorescent Nucleotides and Vanadate, *J. Biochem. (Tokyo) 96*, 147−154.
11. Fisher, A. J., Smith, C. A., Thoden, J. B., Smith, R., Sutoh, K., Holden, H. M., and Rayment, I. (1995) X-ray Structures of the Myosin Motor Domain of *Dictyostelium discoideum* Complexed with MgADP·BeF_x and MgADP·AlF_4^-, *Biochemistry 34*, 8960−8972.
12. Rayment, I., Rypniewski, W. R., S.-Bäse, K., Smith, R., Tomchick, D. R., Benning, M. M., Winkelmann, D. A., Wesenberg, G., and Holden, H. M. (1993) Three-Dimensional Structure of Myosin Subfragment-1: A Molecular Motor, *Science 261*, 50−58.
13. Bauer, C. B., Holden, H. M., Thoden, J. B., Smith, R., and Rayment, I. (2000) X-ray Structures of the Apo and MgATP-bound States of *Dictyostelium discoideum* Myosin Motor Domain, *J. Biol. Chem. 275*, 38494−38499.
14. Dewar, M. J. S., Zoebisch, E. G., Healy, E. F., and Stewart, J. P. (1985) Development and use of quantum mechanical molecular models. 76. AM1: a new general purpose quantum mechanical molecular model, *J. Am. Chem. Soc. 107*, 3902−3909.
15. Goodno, C. C. (1979) Inhibition of myosin ATPase by vanadate ion, *Proc. Natl Acad. Sci. U.S.A. 76*, 2620−2624.
16. Viola, R. E., Morrison, J. F., and Cleland, W. W. (1980) Interaction of Metal(III)- Adenosine 5′-Triphosphate Complexes with Yeast Hexokinase, *Biochemistry 19*, 3131−3137.
17. Morrison, J. F. (1982) The slow-binding and slow, tight-binding inhibition of enzyme-catalysed reactions, *TIBS 7*, 102−105.
18. Lancet, D., and Pecht, I. (1977) Spectroscopic and Immunochemical Studies with Nitrobenzoxadiazolealanine, a Fluorescent Dinitrophenyl Analogue, *Biochemistry 16*, 5150−5157.
19. Collini, M., Alfonso, L. D., Molinari, H., Ragona, L., Catalano, M., and Baldini, G. (2003) Competitive binding of fatty acids and the fluorescent probe 1-8-anilinonaphthalene sulfonate to bovine β-lactoglobulin, *Protein Sci. 12*, 1596−1603.
20. Thumser, A. E. A., Buckland, A. G., and Wilton, D. C. (1998) Monoacylglycerol binding to human serum albumin: Evidence that monooleoylglycerol binds at the dansylsarcosine site, *J. Lipid Res. 39*, 1033−1038.
21. Kontopidis, G., Holt, C., and Sawyer, L. (2002) The Ligand-binding Site of Bovine β-Lactoglobulin: Evidence for a Function?, *J. Mol. Biol. 318*, 1043−1055.
22. Bhattacharya, A. A., Grüne, T., and Curry, S. (2000) Crystallographic Analysis Reveals Common Modes of Binding of Medium and Long-chain Fatty Acids to Human Serum Albumin, *J. Mol. Biol. 303*, 721−732.
23. Werber, M. M., Szent-Györgyi, A. G., and Fasman, G. D. (1972) Fluorescence Studies on Heavy Meromyosin-Substrate Interaction, *Biochemistry 11*, 2872−2883.
24. Hiratsuka, T. (1992) Spatial Proximity of ATP-sensitive Tryptophanyl Residue(s) and Cys-697 in Myosin ATPase, *J. Biol. Chem. 267*, 14949−14954.
25. Papp, S., and Highsmith, S. (1993) The ATP−Induced Myosin Subfragment-1 Fluorescence Intensity Increase Is Due to One Tryptophan, *Biochim. Biophys. Acta 1202*, 169−172.
26. Batra, R., and Manstein, D. J. (1999) Functional characterisation of Dictyostelium myosin II with conserved tryptophanyl residue 501 mutated to tyrosine, *Biol. Chem. 380*, 1017−1023.
27. Park, S., and Burghardt, T. P. (2000) Isolating and Localizing ATP-Sensitive Tryptophan Emission in Skeletal Myosin Subfragment 1, *Biochemistry 39*, 11732−11741.
28. Yengo, C. M., Chrin, L. R., Rovner, A. S., and Berger, C. L. (2000) Tryptophan 512 Is Sensitive to Conformational Changes in the Rigid Relay Loop of Smooth Muscle Myosin during the MgATPase Cycle, *J. Biol. Chem. 275*, 25481−25487.
29. Onishi, H., Konishi, K., Fujiwara, K., Hayakawa, K., Tanokura, M., Martinez, H. M., and Morales, M. F. (2000) On the tryptophan residue of smooth muscle myosin that responds to binding of nucleotide, *Proc. Natl. Acad. Sci. U.S.A. 97*, 11203−11208.
30. Dominguez, R., Freyzon, Y., Trybus, K. M., and Cohen, C. (1998) Crystal Structure of a Vertebrate Smooth Muscle Myosin Motor Domain and Its Complex with the Essential Light Chain: Visualization of the Pre-Power Stroke State, *Cell 94*, 559−571.
31. Geeves, M. A. and Holmes, K. C. (1999) Structural Mechanism of Muscle Contraction, *Annu. Rev. Biochem. 68*, 687−728.
32. Kovács, M., Tóth, J., Hetényi, C., M.-Csizmadia, A., and Sellers, J. R. (2004) Mechanism of Blebbistatin Inhibition of Myosin II, *J. Biol. Chem. 279*, 35557−35563.

BI051373L